

Stochastic Shape Optimization via Design-Space Augmented Dimensionality Reduction and RANS Computations

Andrea Serani* and Matteo Diez†

CNR-INM, National Research Council-Institute of Marine Engineering
Via di Vallerano 139, 00128 Rome, Italy

Jeroen Wackers‡ and Michel Visonneau§

LHEEA Lab, Ecole Centrale de Nantes, CNRS UMR 6598
1 rue de la Noe, 44321 Nantes, Cedex 3, France

Frederick Stern¶

IIHR-Hydroscience and Engineering, The University of Iowa
100 C. Maxwell Stanley Hydraulics Laboratory, Iowa City, Iowa 52242-1585, USA

The paper presents how to efficiently and effectively solve stochastic shape optimization problems by combining Reynolds-averaged Navier-Stokes (RANS) equation solvers with design-space augmented dimensionality reduction (ADR). This study has been conducted within the NATO Science and Technology Organization, Applied Vehicle Technology, Task Group AVT-252 “Stochastic Design Optimization for Naval and Aero Military Vehicles.” The application pertains to the robust and the reliability-based robust design optimization of a destroyer hull-form for resistance in calm water and waves and seakeeping performance, under stochastic environmental and operating conditions (speed, sea state, heading). The current work extends previous research by the authors, presented at earlier AIAA conferences [1–3], where only potential flow solvers were used. In the present work, the expected value of the total resistance is reduced respectively by 4.4 and 3% in calm water and waves. An 8% improvement of the seakeeping performance is also achieved. Design-space assessment by ADR is demonstrated to be a viable option in solving the curse of dimensionality in shape optimization, especially when high-fidelity CPU-expensive solvers are used.

I. Introduction

The simulation-based design (SBD) paradigm is rapidly replacing the traditional build-and-test design approach for naval and aeronautical military vehicles, offering innovative out-of-the-box design opportunities previously not realizable due to technological limitations. The recent and continuous improvement of high-performance computing (HPC) systems has allowed the application of high-fidelity simulation tools and the integration of optimization algorithms in the SBD process, leading to effective, efficient, and automatic SBD optimization (SBDO) procedures. In single/multi-disciplinary shape optimization, SBDO consists of three main elements: (i) performance analysis, (ii) optimization algorithm, and (iii) geometry modification and automatic meshing tool (see Fig. 1, right box).

Real world applications of SBDO are affected by uncertainties and require both an accurate modeling of environmental and operating conditions, and the solution of an uncertainty quantification (UQ) problem within the performance analysis and the optimization loop. Robust and/or reliability-based design optimization formulations are required to integrate UQ and the associated statistical estimators into the design process. Despite the availability of powerful HPC systems, SBDO for shape optimization under stochastic conditions still remains a challenging process, from theoretical, algorithmic, and technological viewpoints, especially when high-fidelity solvers are used.

In the optimization process, design improvements depend strongly on the dimension and the extent of the design space. The curse of dimensionality is relevant in simulation-based shape optimization, especially when complex physics

*Postdoctoral Research Fellow, andrea.serani@insean.cnr.it

†Research Scientist, AIAA Member, matteo.diez@cnr.it

‡Research Scientist, jeroen.wackers@ec-nantes.fr

§Research Director, michel.visonneau@ec-nantes.fr

¶Professor, Dept. of Mechanical Engineering, frederick.stern@uiowa.edu

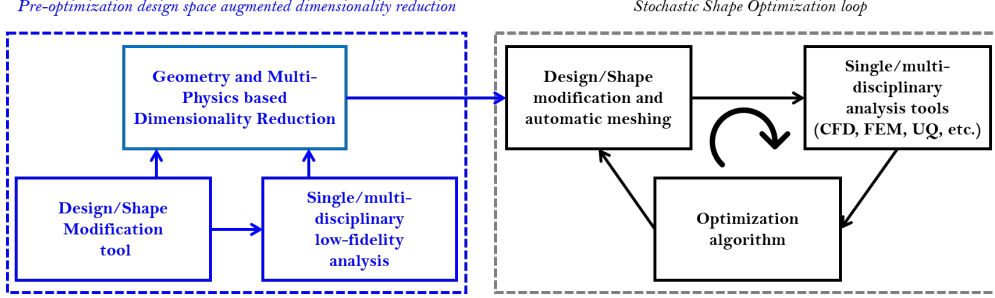


Fig. 1 SBDO scheme, including pre-optimization (offline) design-space augmented dimensionality reduction based on low-fidelity solvers.

and high-fidelity computationally-expensive solvers are involved in the process and a global optimum is sought after. On the one hand, high-dimensional and high variability spaces offer more margins of improvement, on the other hand they are more difficult and computationally expensive to be explored. The assessment of the design space and the breakdown of its variability therefore are key elements to increase the efficiency of an SBDO procedure [4].

Offline dimensionality reduction (DR) techniques have been developed to limit design-space variability for efficient analysis and optimization procedures [5, 6]. A method based on the generalized Karhunen-Loëve expansion (KLE, equivalent to a generalized proper orthogonal decomposition, POD) has been formulated to define a reduced-dimensionality global model of the design space, which conserves a prescribed level of variability of the geometry [4]. No objective function evaluation nor gradient is required by the method. The method has been successfully applied for deterministic [1, 7, 8] and stochastic [9, 10] hull form optimization of monohulls and catamarans in calm water and waves, respectively. Similarly, Poole et al. [11] have applied POD to airfoil shape optimization via singular value decomposition (SVD) of an airfoil geometric-data library. Offline methods improve the shape optimization efficiency by reparametrization and DR, using an assessment of the design space and the shape parametrization before optimization and/or design performance analysis are performed. The assessment is based on the geometric variability associated with the design space for the shape optimization. Lately, Diez et al. [12] have extended (augmented) the DR based on KLE, combining geometry modification vectors with associated physics-based vectors by an offline variable-fidelity formulation of the design-space DR problem. The design-space augmented dimensionality reduction (ADR) was applied to deterministic [1], robust [2], and reliability-based robust [3] shape optimization, but limited to low fidelity solvers.

The objective of the present work is to show how design-space ADR can lead to an efficient and accurate shape optimization procedure, by application of high-fidelity computational fluid dynamics (CFD) solvers. The current work is an extension of earlier research by the authors [1–3] where only low-fidelity solvers were used.

This paper shows the RANS (Reynolds-averaged Navier-Stokes) based optimization of a naval destroyer, namely the DTMB 5415 model, for improved resistance in calm water and waves and seakeeping under stochastic environmental and operating conditions including variable speed, sea state, and heading. Both robust design optimization (RDO) and reliability-based robust design optimization (RBRDO) problems are solved. The results are part of the research conducted by the ECN/CNRS and CNR-INM teams within the NATO Science and Technology Organisation, Applied Vehicle Technology, Task Group AVT-252 “Stochastic Design Optimization for Naval and Aero Military Vehicles.”

The paper is organized as follows. Section II presents the design-space augmented dimensionality reduction method at the basis of the current study. Section III presents the CFD solvers used in the current study. Section IV outlines the formulation of the stochastic shape optimization problems with the underlying assumptions. The numerical results are presented in Section V, whereas conclusions are discussed in Section VI.

II. Design-Space Augmented Dimensionality Reduction

Consider the shape modification vector $\delta \in \mathbb{R}^{m_1}$, $m_1 = 1, \dots, 3$ which is defined on a manifold $\mathcal{G} \in \mathbb{R}^n$ (the geometry), along with a distributed physical parameter vector $\pi \in \mathbb{R}^{m_2}$, $m_2 = 1, \dots, \infty$ (representing, e.g., velocity, pressure distribution, wave elevation, etc.) that is defined on the flow domain $\mathcal{P} \in \mathbb{R}^n$. Finally, a lumped (or global) physical parameter vector is defined as $\theta \in \mathbb{R}^{m_3}$, $m_3 = 1, \dots, \infty$ (representing, e.g., ship resistance, motion RMS, etc.) on a domain \mathcal{Q} . Note that \mathcal{Q} has a null measure and corresponds to an arbitrary point where the lumped physical parameter vector is virtually defined. Also note that, in general, $\mathcal{D} \equiv \mathcal{G} \cup \mathcal{P} \cup \mathcal{Q}$ is not simply connected. Rather, \mathcal{G} may

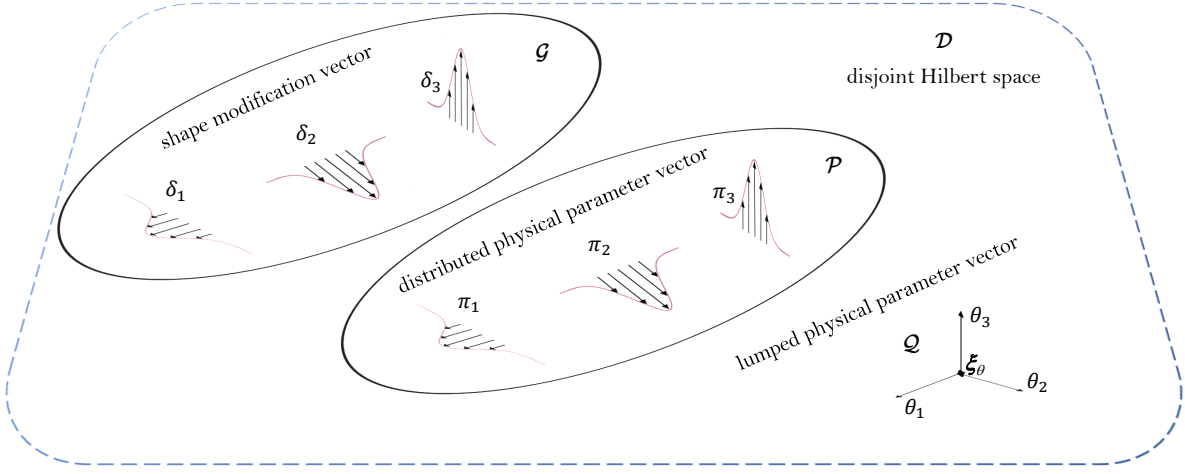


Fig. 2 Domains for shape modification vector, distributed physical parameter vector, and lumped (or global) physical parameter vector in a disjoint Hilbert space.

be a boundary of \mathcal{P} . Figure 2 summarizes these domains and vectors.

Finally, assume that the shape modification of the geometry is governed by the design parameters $\mathbf{u} \in \mathbb{R}^M$, which have a domain \mathcal{U} . The objective of the following KLE analysis is to isolate new design parameters which have a maximum influence on δ , π and θ , so that most of the design variability can be expressed with fewer than M parameters.

Consider now a combined geometry and multi-physics based vector $\gamma \in \mathbb{R}^m$, where the physics part may contain multi-disciplinary information. For the sake of simplicity, consider one set of coordinates $\xi \in \mathbb{R}^n$, such that

$$\gamma(\xi, \mathbf{u}) = \begin{cases} \delta(\xi, \mathbf{u}) & \text{if } \xi \in \mathcal{G} \\ \pi(\xi, \mathbf{u}) & \text{if } \xi \in \mathcal{P} \\ \theta(\xi, \mathbf{u}) & \text{if } \xi \in \mathcal{Q} \end{cases} \quad (1)$$

as belonging to a disjoint Hilbert space $L^2_{\rho}(\mathcal{D})$, defined by the generalized inner product

$$(\mathbf{a}, \mathbf{b})_{\rho} = \int_{\mathcal{D}} \rho(\xi) \mathbf{a}(\xi) \cdot \mathbf{b}(\xi) d\xi = \int_{\mathcal{G}} \rho(\xi) \mathbf{a}(\xi) \cdot \mathbf{b}(\xi) d\xi + \int_{\mathcal{P}} \rho(\xi) \mathbf{a}(\xi) \cdot \mathbf{b}(\xi) d\xi + \rho(\xi_{\theta}) \mathbf{a}(\xi_{\theta}) \cdot \mathbf{b}(\xi_{\theta}) \quad (2)$$

with associated norm $\|\mathbf{a}\| = (\mathbf{a}, \mathbf{a})_{\rho}^{\frac{1}{2}}$, where $\rho(\xi) \in \mathbb{R}$ is an arbitrary weight function. Note that in general, one may have multi-disciplinary physics vectors defined over multiple different domains, $\mathcal{P}_1, \dots, \mathcal{P}_{\infty}$. In this case, $\mathcal{P} \equiv \bigcup_{k=1}^{\infty} \mathcal{P}_k$. Considering the design modification vector only, generally, $\xi \in \mathbb{R}^n$ with $n = 1, 2, 3$ and $\delta \in \mathbb{R}^m$ with $m = 1, 2, 3$ (with m not necessarily equal to n). For example, a typical hull geometry is a curved surface in three dimensions, so it has $n = 2$ and $m \leq 3$ (meaning that the shape modification vector has at most three components). Figure 3 shows an example with $n = 1$ and $m = 2$, for the design modification vector $\delta(\xi, \mathbf{u})$.

Give the design vector \mathbf{u} an arbitrary probability density function $p(\mathbf{u})$. Considering all possible realizations of \mathbf{u} , the associated mean vector is

$$\langle \gamma \rangle(\xi) = \int_{\mathcal{U}} \gamma(\xi, \mathbf{u}) p(\mathbf{u}) d\mathbf{u} \quad (3)$$

Where $\langle \cdot \rangle$ denotes the ensemble average over \mathbf{u} . The associated variance (considering globally combined geometry and multi-physics based variability) equals

$$\sigma^2 = \langle \|\hat{\gamma}\|^2 \rangle = \int_{\mathcal{U}} \int_{\mathcal{D}} \rho(\xi) \hat{\gamma}(\xi, \mathbf{u}) \cdot \hat{\gamma}(\xi, \mathbf{u}) p(\mathbf{u}) d\xi d\mathbf{u} \quad (4)$$

where $\hat{\gamma}(\xi, \mathbf{u}) = \gamma(\xi, \mathbf{u}) - \langle \gamma \rangle(\xi)$ represents the combined geometry and multi-physics based modification vector.

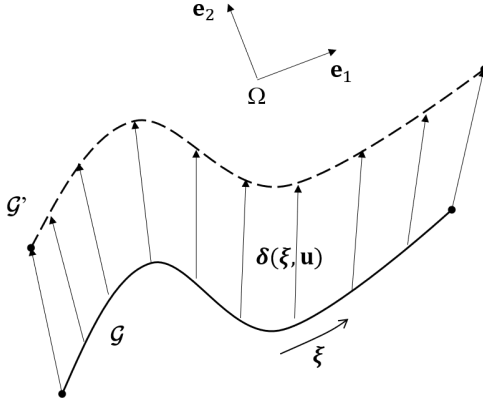


Fig. 3 Scheme and notation for the current formulation, showing an example for $n = 1$ and $m = 2$.

The aim of the KLE is to find an optimal basis of orthonormal functions which will be used to construct a linear, decomposed representation of $\hat{\gamma}$:

$$\hat{\gamma}(\xi, \mathbf{u}) \approx \sum_{k=1}^N x_k(\mathbf{u}) \psi_k(\xi) \quad (5)$$

In order to perform design-space ADR, the basis functions ψ_k in each subdomain of \mathcal{D} is denoted as:

$$\psi_k(\xi) = \begin{cases} \varphi_k(\xi) & \text{if } \xi \in \mathcal{G} \\ \chi_k(\xi) & \text{if } \xi \in \mathcal{P} \\ \nu_k(\xi) & \text{if } \xi \in \mathcal{Q} \end{cases} \quad (6)$$

and

$$x_k(\mathbf{u}) = (\hat{\gamma}, \psi_k)_\rho = \int_{\mathcal{D}} \rho(\xi) \hat{\gamma}(\xi, \mathbf{u}) \cdot \psi_k(\xi) d\xi \quad (7)$$

are the basis-function weights, used hereafter as new design variables that replace \mathbf{u} .

The optimality condition associated with the KLE refers to a maximization of the geometric and multi-physics variance σ retained by the basis functions of Eq. 5. Combining Eqs. 4–7 and using the orthonormality of the basis functions ψ yields:

$$\sigma^2 = \sum_{k=1}^{\infty} \sum_{j=1}^{\infty} \langle x_k x_j \rangle (\psi_k, \psi_j)_\rho = \sum_{k=1}^{\infty} \langle x_k^2 \rangle = \sum_{k=1}^{\infty} \langle (\hat{\gamma}, \psi_k)_\rho^2 \rangle \quad (8)$$

The basis retaining the maximum variance is formed by the solutions ψ_k of the variational problem

$$\begin{aligned} & \underset{\psi \in L_\rho^2(\mathcal{D})}{\text{maximize}} \quad \mathcal{J}(\psi_k) = \langle (\hat{\gamma}, \psi_k)_\rho^2 \rangle \\ & \text{subject to} \quad (\psi_k, \psi_k)_\rho^2 = 1 \end{aligned} \quad (9)$$

which yields [4]

$$\mathcal{L} \psi_k(\xi) = \int_{\mathcal{D}} \rho(\zeta) \langle \hat{\gamma}(\xi, \mathbf{u}) \otimes \hat{\gamma}(\zeta, \mathbf{u}) \rangle \psi_k(\zeta) d\zeta = \lambda_k \psi_k(\xi) \quad (10)$$

where \mathcal{L} is the selfadjoint integral operator whose eigensolutions define the optimal basis functions for the linear representation of Eq. 5. Therefore, its eigenfunctions (KL modes) $\{\psi_k\}_{k=1}^{\infty}$ are orthogonal and form a complete basis for $L_\rho^2(\mathcal{D})$. Additionally (see, e.g., [4])

$$\sigma^2 = \sum_{k=1}^{\infty} \lambda_k \quad (11)$$

where the eigenvalues λ_k (KL values) represent the variance retained by the associated basis function ψ_k , through its component x_k in Eq. 5:

$$\lambda_k = \langle x_k^2 \rangle \quad (12)$$

Finally, the solutions $\{\psi_k\}_{k=1}^{\infty}$ of Eq. 10 are used to build a reduced-dimensionality design space. For efficiency, the eigenmodes are ordered as $\lambda_k \geq \lambda_{k+1}$. Defining l , with $0 < l \leq 1$, as the desired confidence level of the ADR, N in Eq. 5 is selected such as

$$\sum_{k=1}^N \lambda_k \geq l \sum_{k=1}^{\infty} \lambda_k = l\sigma^2 \quad (13)$$

After the design-space ADR is assessed and performed, the geometric components $\{\varphi_k\}_{k=1}^N$ of the eigenvectors ψ_k in Eq. 6 are used for the new representation of the shape modification vector. Details about the numerical implementation of the design-space ADR are given in Serani et al. [2].

Setup and assumptions for current application ADR are provided later in Section IV.E.

III. Computational Fluid Dynamics Solvers

A. ISIS-CFD

The flow solver ISIS-CFD is an incompressible unsteady Reynolds-averaged Navier-Stokes (URANS) method mainly devoted to marine hydrodynamics. The flow solver includes several sophisticated turbulence models available with wall-function or low-Reynolds near wall formulations. The solver is based on the finite volume method to build the spatial discretization of the transport equations. The unstructured discretization is face-based. While all unknown state variables are cell-centered, the systems of equations used in the implicit time stepping procedure are constructed face by face. Fluxes are computed in a loop over the faces and the contribution of each face is then added to the two cells next to the face. This technique poses no specific requirements on the topology of the cells. Therefore, the grids can be completely unstructured; cells with an arbitrary number of arbitrarily-shaped faces are accepted.

Pressure-velocity coupling is enforced through a Rhie & Chow SIMPLE type method [13]: at each time step, the velocity updates come from the momentum equations and the pressure is given by the mass conservation law, transformed into a pressure equation. In the case of turbulent flows, transport equations for the variables in the turbulence model are added to the discretization. Free-surface flow is simulated with a multi-phase flow approach: the water surface is captured with a conservation equation for the volume fraction of water, discretized with specific compressive discretization schemes. The technique included for the 6 degrees of freedom (DoF) simulation of solid body motion is described by [14]. Time-integration of Newton's law for the body motion is combined with analytic weighted or elastic analogy grid deformation to adapt the fluid mesh to the moving ship. Finally, an anisotropic automatic grid refinement procedure has been developed which is controlled by various flow-related criteria [15].

In the present work the wall-function condition is applied on the solid surfaces while far field boundary conditions are imposed on the lateral sides of the computational domain. Pressure is imposed on the top and bottom. A half geometry is simulated with a symmetry condition on the center plane. The $k - \varepsilon$ - SST turbulence model is used.

B. CFDShip-Iowa

CFDShip-Iowa is a URANS code [16], developed at the University of Iowa, IIHR-Hydroscience & Engineering, over the past 25 years. CFDShip-Iowa V4.5 is an incompressible RANS/DES solver designed for ship hydrodynamics. The equations are solved in an inertial coordinate system, either fixed to a ship or other frame moving at constant speed or in the earth system. The free surface is modelled with a single-phase capturing approach, meaning that only the water flow is solved, enforcing kinematic and dynamic free-surface boundary conditions on the interfaces. Arbitrary free-surface topologies can be predicted, with the limitation that pressurized closed air/water packets (bubbles) cannot be simulated. The solver uses structured multiblock grids and has overset capabilities. Other capabilities include 6 DoF motions, several turbulence models, moving control surfaces, multi-objects, advanced controllers, propulsion models, incoming waves and wind, bubbly flow, and fluid-structure interaction [17].

In the present study the URANS equations are solved in the inertial coordinate system fixed to the ship. The turbulence is computed with an isotropic model (Menter's blended $k - \omega/k - \varepsilon$ - BKW) with shear stress transport (SST). A second order upwind scheme is used to discretize the convective terms of the momentum equations. The pressure implicit with splitting of operators (PISO) loop for pressure/velocity coupling is used. For high-performance

parallel computing, an MPI-based domain decomposition approach is used, where each decomposed block is mapped to one processor. The code SUGGAR runs as a separate process from the flow solver to compute interpolation coefficients for the overset grid, which enables CFDShip-Iowa to take care of 6 DoF movement with a motion controller at every time step. Simulations are performed for the right demi-hull for both calm-water and head waves, taking advantage of symmetry about the xz -plane (see Fig. 4).

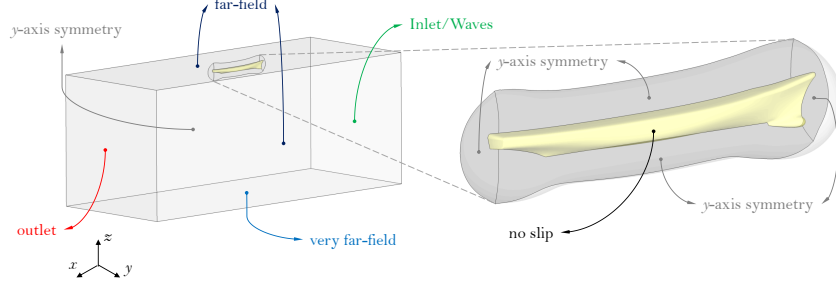


Fig. 4 Summary of boundary conditions for calm water/regular head wave simulations by CFDShip-Iowa.

C. SMP

Seakeeping performance are evaluated by the Standard Ship Motion program (SMP), developed at the David Taylor Naval Ship Research and Development Center [18]. SMP provides a potential flow solution based on linearized strip theory. The 6 DoF response of the ship is given, advancing at constant forward speed with arbitrary heading in both regular waves and irregular seas, as well as the longitudinal, lateral, and vertical responses at specified locations of the ship.

IV. Stochastic Shape Optimization Problem: Destroyer Hull

A. Model Geometry

The DTMB 5415 model is selected as a test case for the current application. It is an open-to-public early concept of the DDG-51 (see Fig. 5), a USS Arleigh Burke-class destroyer, widely used for both towing tank experiments [19] and hull-form SBDO [8]. The main particulars of the DTMB 5415 and the test conditions are summarized in Tab. 1. Since no rudder is considered here, the L_{pp} is calculated from the fore perpendicular to the transom bottom edge.

B. Stochastic Environmental and Operating Conditions

Stochastic conditions are: velocity U from 18kn to 30kn ($0.25 \leq Fr \leq 0.41$) following the transit speed-time distribution (see Fig. 6a), defined using the kernel density estimation (KDE) of 2013 data from Anderson et al. [20], approximated by

$$p(U) = 2(-0.0063715U + 0.192915) \quad (14)$$

Sea state S from 4 to 6 following the probability occurrence of the North Atlantic Ocean (see Fig. 6b [21] and Tab. 2); heading β with respect to the waves from 0 deg to 180 deg following a uniform distribution (see Fig. 6c [22]).

C. Optimization Problem Statement

A single-objective RDO, addressing the the calm water total resistance coefficient minimization, and a multi-objective RBRDO problem, addressing the minimization of the total resistance in waves and the maximization of the ship operability, are solved. Details are provided in the following subsections.

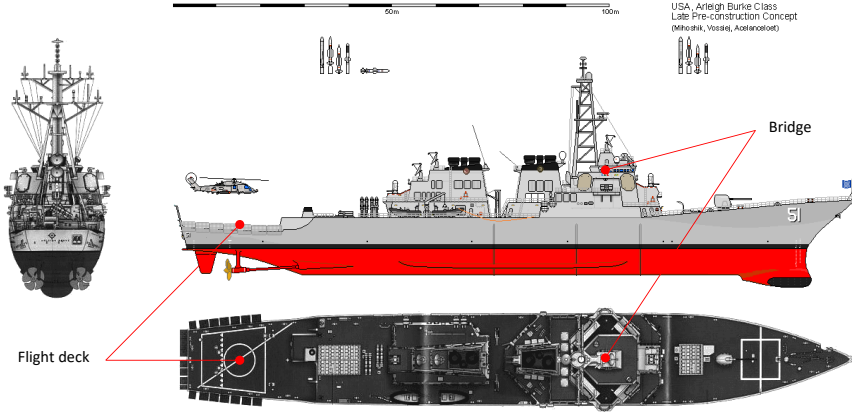


Fig. 5 DDG-51 overview with bridge and flight deck location (images from the-blueprints.com and ship-bucket.com).

Table 1 DTMB 5415 main particulars and fluid conditions.

Description	Symbol	Unit	Full scale	Model scale
Displacement	∇	tonnes	8,437	0.549
Length between perpendiculars	L_{pp}	m	142.0	5.720
Beam	B	m	18.90	0.760
Draft	T	m	6.160	0.248
Longitudinal center of gravity	LCG	m	71.60	2.884
Vertical center of gravity	VCG	m	1.390*	0.056*
Bridge longitudinal position	B_x	m	44.00†	1.772†
Bridge vertical position	B_z	m	24.75‡	0.997‡
Flight deck longitudinal position	D_x	m	132.0†	5.317†
Flight deck vertical position	D_z	m	13.00‡	0.524‡
Roll radius of gyration	K_{xx}	–	0.40B	
Pitch radius of gyration	K_{yy}	–	0.25 L_{pp}	
Yaw radius of gyration	K_{zz}	–	0.25 L_{pp}	
Water density	ρ	kg/m ³	998.5	
Kinematic viscosity	ν	m ² /s	1.09E-6	
Gravity acceleration	g	m/s ²	9.803	

* Above the water line; † Backward bow; ‡ Above the keel; ** ADR conditions

1. Robust Design Optimization in Calm Water

The following single-objective RDO problem is solved:

$$\begin{aligned}
 & \text{minimize} && \mu[C_T(\mathbf{x}, U)] \\
 & \text{subject to} && h_i(\mathbf{x}) = 0, \quad i = 1, \dots, I \\
 & && \text{and to} \quad l_j(\mathbf{x}) \leq 0, \quad j = 1, \dots, J \\
 & && \text{and to} \quad \mathbf{x}_l \leq \mathbf{x} \leq \mathbf{x}_u
 \end{aligned} \tag{15}$$

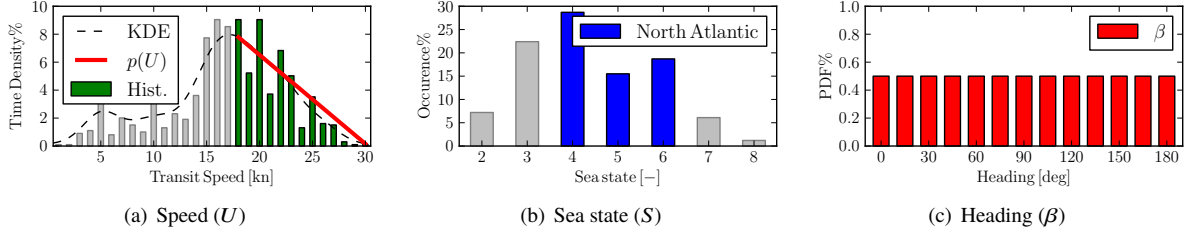


Fig. 6 Stochastic parameters distribution.

Table 2 Annual sea state occurrence in the open North Atlantic Ocean [21].

S	$\hat{p}(S)\%$	$p(S)\%$	$H_{1/3}$ [m]	$p(H_{1/3})\%$	\bar{H} [m]	T_p [s]
≤ 1	0.00	-	0.05	-	0.03	-
2	7.20	-	0.30	-	0.19	7.5
3	22.4	-	0.88	-	0.55	7.5
4	28.7	45.6	1.88	36.5	1.18	8.8
5	15.5	24.6	3.25	16.4	2.04	9.7
6	18.7	29.7	5.00	14.9	3.13	12.4
7	6.10	-	7.50	-	4.70	15.0
8	1.20	-	11.5	-	7.21	16.4
> 8	< 0.05	-	> 14	-	> 8.77	20.0

where \mathbf{x} is the reduced-dimensionality design variable vector, μ is the expected value of the model scale total resistance coefficient (C_T) in calm water at variable speed (U) defined by

$$\mu[C_T(\mathbf{x}, U)] = \int_U C_T(\mathbf{x}, U)p(U)dU \quad (16)$$

where $p(U)$ is the probability density function (PDF) associated to calm water evaluations with variable speed (see Eq. 14). Finally, equality h_i and inequality l_j geometrical constraints include fixed length between perpendiculars (L_{pp}) and displacement (∇), along with a $\pm 5\%$ maximum variation of beam (B) and draft (T), respectively, and reserved volume for the sonar in the dome, corresponding to 4.9 m diameter and 1.7 m length (cylinder).

2. Reliability-based Robust Design Optimization in Waves

The following multi-objective RBRDO is solved:

$$\begin{aligned} & \text{minimize} && \{\mu[\bar{R}_T(\mathbf{x}, U, H_{1/3}, T_p)], -\Omega(\mathbf{x})\}^\top \\ & \text{subject to} && h_i(\mathbf{x}) = 0, && i = 1, \dots, I \\ & && l_j(\mathbf{x}) \leq 0, && j = 1, \dots, J \\ & \text{and to} && \mathbf{x}_l \leq \mathbf{x} \leq \mathbf{x}_u \end{aligned} \quad (17)$$

where μ is the expected value of the model scale mean total resistance (\bar{R}_T) in head waves at variable speed (U) and significant wave height ($H_{1/3}$, representative of the sea state) and Ω is the full scale ship operability considering North Atlantic Ocean conditions with variable speed, wave height, and heading (β). Equality and inequality constraint are defined as per the RDO problem. The objectives are described by Eqs. 18 and 19, respectively

$$\mu[\bar{R}_T(\mathbf{x}, U, H_{1/3}, T_p)] = \iiint_{U, H_{1/3}, T_p} \bar{R}_T(\mathbf{x}, U, H_{1/3}, T_p)p(U, H_{1/3}, T_p)dT_p dH_{1/3} dU \quad (18)$$

$$\Omega(\mathbf{x}) = \iiint_{U, H_{1/3}, T_p, \beta} \bigcap_{n=1}^{N_g} [\text{SSA}_n(\mathbf{x}, U, H_{1/3}, T_p, \beta) \leq \max(\text{SSA}_n)] p(U, H_{1/3}, T_p, \beta) d\beta dT_p dH_{1/3} dU \quad (19)$$

where $p(U, H_{1/3}, T_p)$ is the joint PDF of the stochastic environmental parameter considered; SSA_n are the significant single amplitude operator, representing the seakeeping constraints addressing subsystem seakeeping performance as per NATO STANAG 4154 [22]. These include criteria for mobility, anti-submarine warfare, surface warfare, anti-air warfare, imposing constraints for: roll motion, pitch motion, vertical acceleration at bridge, vertical velocity at flight deck, and wetnesses/slams/emergencies per hour. Here, a limited set of four constraints ($N_g = 4$) is considered, addressing roll and pitch motions, vertical velocity at the flying deck, and vertical acceleration at the bridge, with maximum allowable values summarized in Tab. 3.

Table 3 Subsystem seakeeping performance criteria [22].

Criterion	Unit	Symbol	$\max(\text{SSA})$
Roll motion	deg	SSA_1	8.00
Pitch motion	deg	SSA_2	3.00
Vertical acceleration at bridge	g	SSA_3	0.40
Vertical velocity at flight deck	m/s	SSA_4	0.99

Expected Value of Mean Total Resistance in Irregular Waves: The time-average total resistance in irregular waves is evaluated by regular wave analysis as

$$\bar{R}_T = R_{CW} + \bar{R}_{AW} \quad (20)$$

where R_{CW} is the calm-water total resistance and \bar{R}_{AW} is the average added resistance, predicted from the non-dimensional added resistance response function (C_{AW}) by

$$\bar{R}_{AW} = 2 \int_0^{+\infty} C_{AW} S_\zeta(\omega_e) d\omega_e \quad \text{with} \quad C_{AW} = \frac{\bar{R}_{RW} - R_{CW}}{\zeta_0^2} \quad (21)$$

where ζ_0 is the wave amplitude, ω_e is the wave-encounter frequency, and $S_\zeta(\omega_e)$ is the encounter wave spectrum evaluated from the wave spectrum $S_\zeta(\omega)$ as

$$S_\zeta(\omega_e, U, \beta, H_{1/3}, T_p) = S_\zeta(\omega, H_{1/3}, T_p) \frac{g}{g + 2\omega U \cos \beta} \quad (22)$$

Here, the Bretschneider ocean wave spectrum is considered, defined by

$$S_\zeta(\omega) = \frac{5}{16} \frac{\omega_p^4}{\omega^5} H_{1/3}^2 e^{-5\omega_p^4/4\omega^4} \quad (23)$$

where $\omega_p = 2\pi/T_p$ is the peak angular frequency. Figure 7 shows the Bretschneider spectra for sea state 4, 5, and 6 for the North Atlantic Ocean (see Tab. 2).

Combining Equations 20 and 21, Equation 16 can be recast as

$$\begin{aligned} \mu[\bar{R}_T(\mathbf{x}, U, H_{1/3}, T_p)] &= \\ &= \int_U R_{CW}(\mathbf{x}, U) p(U) dU + 2 \iint_{U, H_{1/3}} \left[\int_{\omega_e} C_{AW}(\mathbf{x}, U, H, \omega_e) S_\zeta(\omega_e, U, H_{1/3}, T_p(H_{1/3})) d\omega_e \right] p(U, H_{1/3}) dH_{1/3} dU \end{aligned} \quad (24)$$

with $H = \tilde{H} = \sqrt{\pi/8} H_{1/3}$.

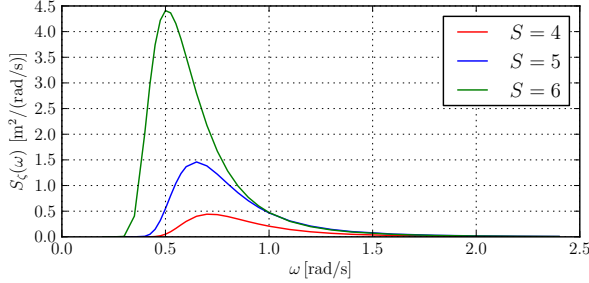


Fig. 7 Bretschneider North Atlantic sea spectra.

Operability: The operability (or ship motion) constraints are related to the SSA of roll and pitch motions, vertical velocity at the flying deck, and vertical acceleration at the bridge. The SSA of the generic χ -motion is defined as

$$\text{SSA}(\chi) = 2\sqrt{m_\chi} \quad (25)$$

where m_χ is the spectral moment (standard deviation, STD or root mean square, RMS) of the generic motion χ . In a probabilistic form the general spectral moment m_χ reads

$$m_\chi = \mathbb{E}[q(\omega_e)] = \int_0^{+\infty} q(\omega_e)p(\omega_e)d\omega_e \quad (26)$$

with

$$q(\omega_e) = m_\zeta \frac{\sigma_\chi^2(\omega_e)}{\zeta_0^2} \quad \text{and} \quad p(\omega_e) = \frac{S_\zeta(\omega_e)}{m_\zeta} \quad (27)$$

where m_ζ is the area underlined by the encounter wave spectrum

$$m_\zeta = \int_{-\infty}^{+\infty} S_\zeta(\omega_e)d\omega_e \quad (28)$$

and σ_χ is the STD or RMS (if the signal has zero mean) of the χ -motion, evaluated as

$$\sigma_\chi = \sqrt{\frac{1}{T_2 - T_1} \int_{T_1}^{T_2} [\chi(t) - \bar{\chi}]^2 dt} \quad (29)$$

Combining Eqs. 25, 26, and 27 with 19, the latter can be recast as

$$\Omega(\mathbf{x}) = \iiint_{U, H_{1/3}, \beta} \mathcal{B}(\mathbf{x}, U, H_{1/3}, T_p(H_{1/3}), \beta) p(U, H_{1/3}, \beta) d\beta dH_{1/3} dU \quad (30)$$

with

$$\mathcal{B} = \bigcap_{n=1}^{N_g} \left\{ 2 \left(\int_0^{+\infty} \frac{\sigma_n^2(\mathbf{x}, U, H, \beta, \omega_e)}{\zeta_0^2} S_\zeta(\omega_e, U, \beta, H_{1/3}, T_p(H_{1/3})) d\omega_e \right)^{\frac{1}{2}} \leq \max(\text{SSA}_n) \right\} \quad (31)$$

D. Uncertainty Quantification Methods

1. Non-intrusive probabilistic collocation

For the RDO problem, UQ is performed using the non-intrusive probabilistic collocation method as developed by Wunsch et al. [23] based on the work by Loeven et al. [24]. In this approach, the dependence of a simulation result on a stochastic parameter is obtained with a Lagrange interpolating polynomial that is fitted through the results of deterministic simulations. The collocation points chosen for these simulations correspond to the Gauss quadrature points for general PDF shapes. This has the advantage that arbitrary PDF types can be used to describe the uncertainty.

2. Gaussian Quadrature

An n -point Gaussian quadrature rule is constructed to yield an exact result for polynomials of degree $2n - 1$ or less by a suitable choice of the points x_i and weights w_i for $i = 1, \dots, n$. The domain of integration for such a rule is conventionally taken as $[-1, 1]$, so the rule is stated as

$$\int_{-1}^1 f(x) dx = \sum_{i=1}^n w_i f(x_i) \quad (32)$$

where w_i are weights. Equation 32 can be easily extended to multidimensional integral.

Herein, the Gauss-Legendre quadrature with $n = 2$ for each stochastic variable (weights $w_i = 1$ and Gauss points $x_{1,2} = \pm 1/\sqrt{3}$) is used to approximate Eq. 24 as

$$\begin{aligned} \mu[\bar{R}_T(\mathbf{x}, U, H_{1/3}, T_p)] &= \\ &= \frac{U_u - U_l}{2} \sum_{i=1}^2 R_{CW}(\mathbf{x}, U_i) p(U_i) + \frac{(U_u - U_l)(H_{1/3,u} - H_{1/3,l})}{4} \sum_{i=1}^2 \sum_{j=1}^2 \bar{R}_{AW}(\mathbf{x}, U_i, H_{1/3,j}) p(U_i, H_{1/3,j}) \end{aligned} \quad (33)$$

with

$$\bar{R}_{AW}(\mathbf{x}, U_i, H_{1/3,j}) = (\omega_{e,u,ij} - \omega_{e,l,ij}) \sum_{k=1}^2 C_{AW}(\mathbf{x}, U_i, \bar{H}_j, \omega_{e,ijk}) S_\zeta(U_i, H_{1/3,j}, T_p(H_{1/3,j}), \omega_{e,ijk}) \quad (34)$$

The Gauss points selected for the URANS simulations are summarized in Tab. 4.

Table 4 Stochastic variables used as Gauss points for the RBRDO solution.

i	j	k	Speed			Sea state			
			U [kn]	Fr [-]	Re [-]	$H_{1/3}$ [m]	\bar{H} [m]	$T_p(H_{1/3})$ [s]	ω [rad/s]
1	1	1	20.5	0.283	1.11E+7	2.254	1.412	8.80	0.500
1	1	2	20.5	0.283	1.11E+7	2.254	1.412	8.80	0.770
1	2	1	20.5	0.283	1.11E+7	4.996	3.131	12.4	0.390
1	2	2	20.5	0.283	1.11E+7	4.996	3.131	12.4	0.670
2	1	1	27.5	0.379	1.49E+7	2.254	1.412	8.80	0.560
2	1	2	27.5	0.379	1.49E+7	2.254	1.412	8.80	0.780
2	2	1	27.5	0.379	1.49E+7	4.996	3.131	12.4	0.405
2	2	2	27.5	0.379	1.49E+7	4.996	3.131	12.4	0.710

3. Metamodel-based Importance Sampling

A stochastic radial basis functions (SRBF, [25]) network is used for the prediction of the motions SSA for the solution of the RBRDO problem. Herein, the metamodel prediction (\widetilde{SSA}) is defined as the expected value of 100 RBF metamodels as

$$\widetilde{SSA}(\mathbf{y}) = \mu[h(\mathbf{y}, \epsilon_j)] \quad \text{with} \quad \{\epsilon_j\}_{j=1}^{100} \sim \text{unif}[1, 3] \quad (35)$$

where $\mathbf{y} = \{U, H_{1/3}, \beta\}$ define the stochastic parameters space and

$$h(\mathbf{y}, \epsilon_j) = \sum_{i=1}^{N_T} w_i \varphi \|\mathbf{y} - \mathbf{z}_i\|^{\epsilon_j} \quad (36)$$

with N_T the number of training points and $\mathbf{w} = \{w_i\}$ is the solution of the linear system that provides exact prediction at $\mathbf{y} = \mathbf{z}_i$

$$\mathbf{Aw} = \mathbf{l} \quad \text{with} \quad a_{ij} = \varphi \|\mathbf{z}_i - \mathbf{z}_j\|^{\epsilon_j} \quad \text{and} \quad \mathbf{l} = \{l_i\} \quad (37)$$

The motion constraints are evaluated by the linearized strip theory SMP at the training points, given by the full factorial combination of $U = \{18, 20, 22, 24, 26, 28, 30\}$ kn, $H_{1/3} = \{1.88, 3.25, 5.00\}$ m, and $\beta = \{0, 15, 30, 45\}$,

$60, 75, 90, 105, 120, 135, 150,$
 $165, 180\}$ deg, for a total of $N_T = 273$.

The operability in Eq. 30 is evaluated by importance sampling as

$$\Omega(\mathbf{x}) = \iiint_{U, H_{1/3}, \beta} \frac{\mathcal{B}(\mathbf{x}, U, H_{1/3}, T_p(H_{1/3}), \beta) p(U, H_{1/3}, \beta)}{q(U, H_{1/3}, \beta)} q(U, H_{1/3}, \beta) d\beta dH_{1/3} dU \quad (38)$$

with $q(U, H_{1/3}, \beta)$ the importance distribution. Herein Eq. 38 is solved by a uniform Monte Carlo (MC) sampling over the stochastic parameters space, leading to its discretized form

$$\Omega(\mathbf{x}) \approx \frac{\sum_{i=1}^{N_U} \sum_{j=1}^{N_{H_{1/3}}} \sum_{k=1}^{N_\beta} \bigcap_{n=1}^4 [\widetilde{\text{SSA}}_n(\mathbf{x}, U_i, H_{1/3,j}, \beta_k) \leq \max(\text{SSA}_n)] p(U_i, H_{1/3,j}, \beta_k)}{\sum_{i=1}^{N_U} \sum_{j=1}^{N_{H_{1/3}}} \sum_{k=1}^{N_\beta} p(U_i, H_{1/3,j}, \beta_k)} \quad (39)$$

where $N_U = N_{H_{1/3}} = N_\beta = 25$ are the number of MC samples, composed by speeds, wave heights (sea states), and headings, respectively. MC samples are provided by the SRBF prediction.

E. Design-Space Augmented Dimensionality-Reduction Setup and Assumptions

The design variability vector γ (Eq. 1) contains: a shape modification vector δ based on a three-dimensional orthogonal basis function (OBF) [8] as described in the following Sec. IV.F; a distributed physical parameter vector π that includes the pressure distribution p and wave elevation η ; and a lumped physical parameter vector θ that includes the wave resistance coefficient in calm water C_w and the RMS of vertical acceleration at the bridge a_z and pitch angle ϑ in waves. The design-space ADR is performed considering multiple speeds ($\text{Fr} = 0.25, 0.33, \text{ and } 0.41$), for both calm water and seakeeping performance. The latter are evaluated in head waves at sea state 5. Further details can be found in [3].

F. Hull-Form Modification Method

The original shape modifications $\delta(\xi, \mathbf{u})$ (defining the original design space) are produced directly on the Cartesian coordinates ξ of the computational body surface \mathbf{g} , as per

$$\mathbf{g}(\xi, \mathbf{u}) = \mathbf{g}_0(\xi) + \delta(\xi, \mathbf{u}) \quad (40)$$

where \mathbf{g}_0 represents the original body surface.

The shape modification is defined using $M = 27$ functions of the Cartesian coordinates over a hyper-rectangle embedding the demi hull [8]

$$\boldsymbol{\phi}_i(\xi) : \mathcal{V} = [0, L_{\xi_1}] \times [0, L_{\xi_2}] \times [0, L_{\xi_3}] \in \mathbb{R}^3 \longrightarrow \mathbb{R}^3 \quad (41)$$

with $i = 1, \dots, M$, as

$$\delta(\xi, \mathbf{u}) = \sum_{i=1}^M u_i \boldsymbol{\phi}_i(\xi) \quad (42)$$

where the coefficients $u_i \in \mathbb{R}$ ($i = 1, \dots, M$) are the original design variables and

$$\boldsymbol{\phi}_i(\xi) := \prod_{j=1}^3 \sin \left(\frac{c_{ij}\pi\xi_j}{L_{\xi_j}} + r_{ij} \right) \mathbf{e}_{q(i)} \quad (43)$$

imposing the following orthogonality property:

$$\int_{\mathcal{V}} \boldsymbol{\phi}_i(\xi) \cdot \boldsymbol{\phi}_k(\xi) d\xi = \delta_{ik} \quad (44)$$

In Eq. 43, $\{c_{ij}\}_{j=1}^3 \in \mathbb{R}$ define the order of the function in the corresponding geometric directions ξ ; $\{r_{ij}\}_{j=1}^3 \in \mathbb{R}$ are the corresponding spatial phases; $\{L_{\xi_j}\}_{j=1}^3$ are the hyper-rectangle edge lengths; $\mathbf{e}_{q(i)}$ is a unit vector. Modifications are applied in ξ_1 , ξ_2 , or ξ_3 direction, with $q(i) = 1, 2$, or 3 respectively. The parameter values used here are taken from Serani et al. [8].

Fixed L_{pp} and ∇ are satisfied by automatic geometric scaling, while geometries exceeding the constraints for B and T are discarded. This is used here, since the relationship between beam/draft variations and design variables is not explicitly provided by the orthogonal expansion and geometric scaling.

The reduced-dimensionality space is built as

$$\mathbf{g}(\xi, \mathbf{x}) = \mathbf{g}_0(\xi) + \hat{\delta}(\xi, \mathbf{x}) \quad (45)$$

with

$$\hat{\delta}(\xi, \mathbf{x}) = \sum_{k=1}^N x_k \varphi_k(\xi) \quad (46)$$

where $\{\varphi_k(\xi)\}_{k=1}^N$ are the N geometry eigenvector component of Eq. 6, that cover at least the 95% of the original design variability as per Eq. 13, and $-\sqrt{3\lambda_k} \leq x_k \leq \sqrt{3\lambda_k}$ are the new design variables.

V. Numerical Results

A. Design-Space Augmented Dimensionality Reduction

In the current analysis, the vector spaces are normalized so that the variance associated with the geometry, the distributed and the lumped multi-physics parameter vectors is the same. The weight $\rho(\xi)$ of the grid nodes above the water line is set equal to zero. A number of $S = 9,000$ random designs are produced assuming a uniform distribution $p(\mathbf{u})$ and assessed by low fidelity solvers. Calm water performance are assessed by the linear potential flow solver WARP [26], whereas seakeeping performance are assessed by SMP. Details can be found in [3]. Figure 8 shows the geometry and multi-physics based variability associated with the design space. The PDF is shown for normalized geometric variation $\delta(\xi_2)/L_{pp}$ of a point on the hull, variation of the wave resistance coefficient ΔC_w , variation of the normalized pressure distribution $\Delta p/p_0$ (where p_0 is the pressure reference), variation of the normalized wave elevation $\Delta \eta/L_{pp}$ of a point downstream, variation of the pitch angle $\Delta \theta$, and finally variation of the bridge vertical acceleration Δa_z . Multi-physics PDF are shown conditional to the Froude number.

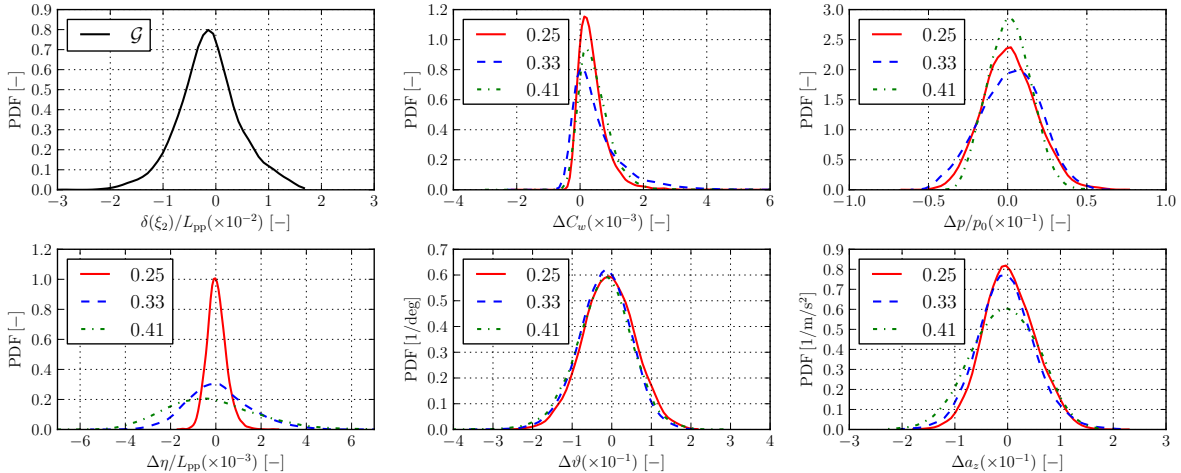


Fig. 8 PDF of geometry and multi-physics based variables associated to the design space variability, using $S = 9,000$ random designs. The multiphysics graphs show curves for three Froude numbers.

Figure 9 shows the KLE results in terms of design variability associated to a reduced-dimensionality space of dimension N for $S = 2,250, 4,500$, and $9,000$ samples. The results are found convergent versus S . The 95% of the original design variability is achieved reducing the number of design variables up to 52% ($N = 14$).

The first three KL modes retaining the largest design variability are shown in Fig. 10. Specifically, the absolute value of the corresponding eigenvector component (geometry, pressure distribution, wave elevation, wave resistance coefficient, pitch, and vertical acceleration) are depicted. The multi-physics eigenvector components are shown conditional to the Froude number.

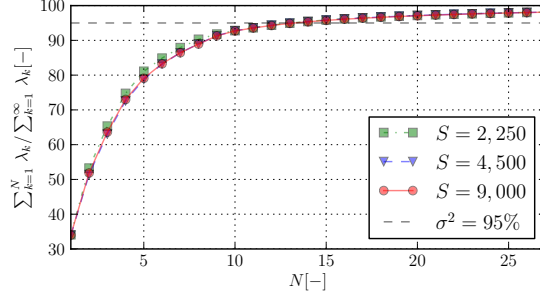


Fig. 9 Normalized variance resolved by reduced-dimensionality spaces of dimension N .

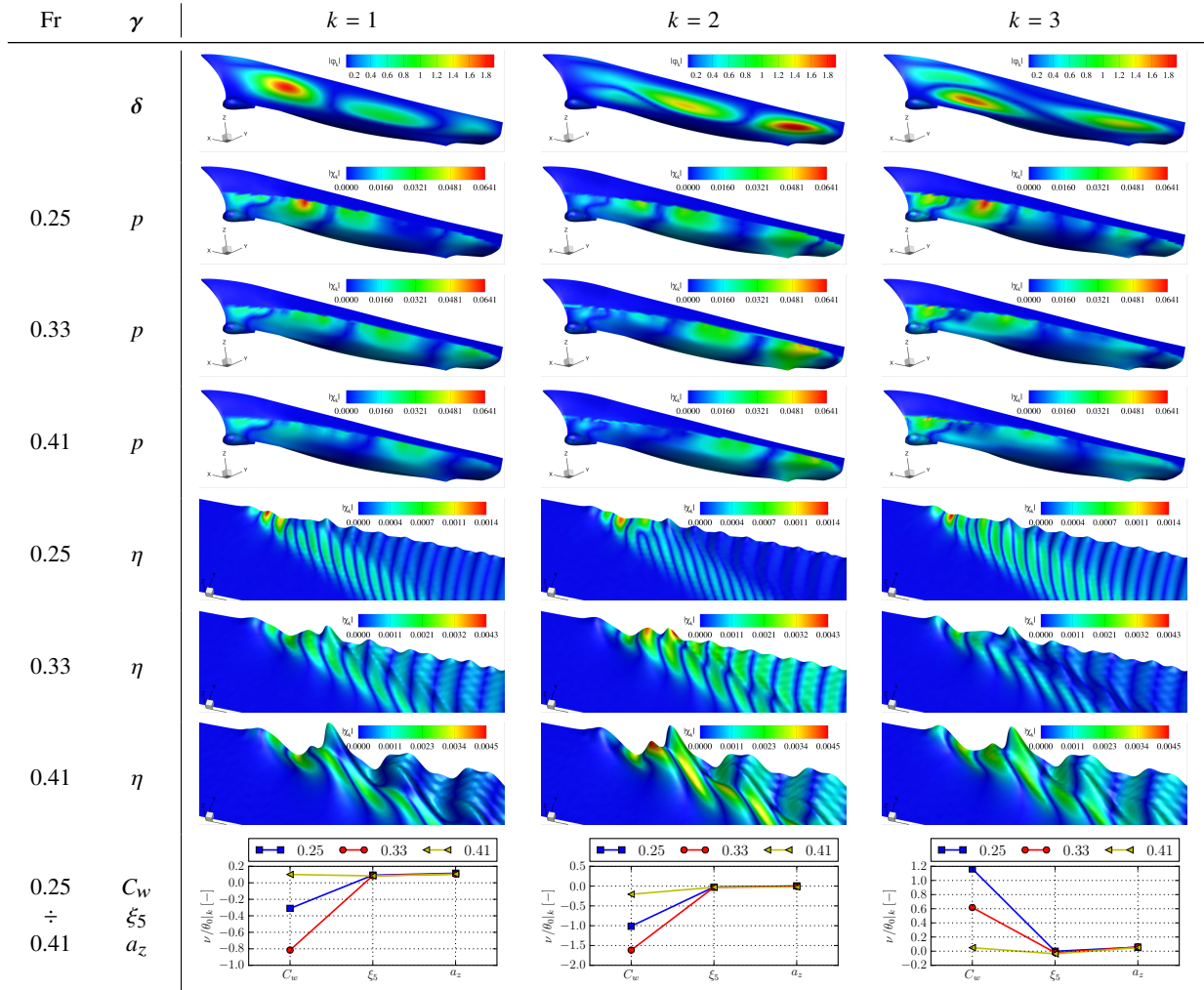


Fig. 10 Geometry and multi-physics eigenvector components.

B. Solution of the RDO Problem in Calm Water

A reduced-dimensionality space resolving about 93% of the original design-space variability is used with $N = 10$. The RDO problem is solved with help of the commercial optimization package FINE/Design3D from NUMECA Int. A design of experiments (DoE) is performed using Latin Hypercube sampling of the design space. A total number of $5N + 1 = 56$ simulations has been performed. Subsequently, optimization is performed using an artificial neural network metamodel approach. In total, 30 design iterations were performed, which corresponds to 90 simulations in

order to perform UQ for each point.

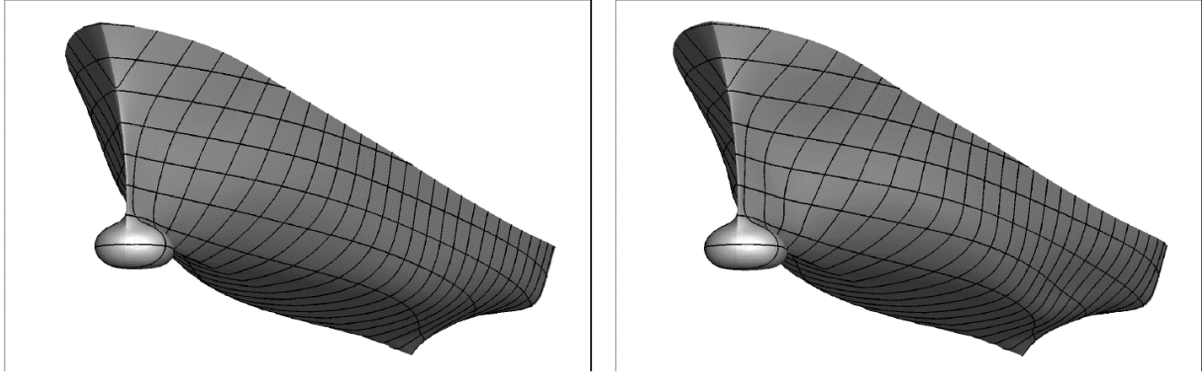


Fig. 11 RDO: baseline (left) and optimal (right) designs.

The optimized geometry is shown in Fig. 11. Compared with the baseline, it has a sharper bow and a notable bulge just behind the bow, which creates a shoulder wave. The midship is thicker than the baseline, whereas the stern has a more slender shape which may produce a smoother pressure recovery and reduce the stern waves. The drag coefficient as a function of the speed is given in Fig. 12: since the velocity probability distribution puts more emphasis on lower speeds, the optimal shape has a reduced total resistance coefficient at low speeds, whereas high-speed performance deteriorates. An average (expected value) total-resistance coefficient reduction of 4% is achieved.

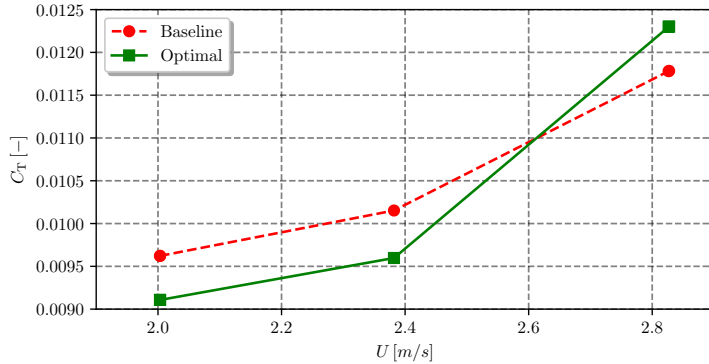


Fig. 12 RDO: dependence of resistance coefficient on the velocity for the optimal and baseline designs.

The wave patterns (see Fig. 13) further clarify why the optimized shape performs better. At the lowest speed, the bow wave is almost completely eliminated by the shoulder wave. The stern wave, which remains unchanged at the lowest velocity, seems a bit smaller than for the baseline at the middle velocity. At this velocity, the shoulder wave is still successful in reducing the bow wave. At the highest velocity on the contrary, the waves have lengthened so the bow and shoulder waves are now in phase. Thus, their amplitudes are summed and the wave resistance increases. Like a bulbous bow on a freighter, the shoulder bulge is a resistance reduction device which is optimal at one speed since it depends on the out-of-phase superposition of two wave systems. The result of performing a robust optimization, instead of a single-speed optimization, is probably that a less pronounced bulge is created. The current results show that the small bulge chosen here is effective for reducing drag over the entire low and middle speed range.

C. Solution of the RBRDO Problem in Waves

A reduced-dimensionality space resolving about 65% of the original design-space variability is used with $N = 3$. Irregular waves total resistance expected value and operability preliminary sensitivity analysis are shown in Fig. 14. The results show a possible improvement of both the objectives. Looking at the design-space isoplanes $x_1 - x_2$ (Fig. 14a and d), $x_1 - x_3$ (Fig. 14b and e), and $x_2 - x_3$ (Fig. 14c and f), the objectives improvement are located at almost opposite

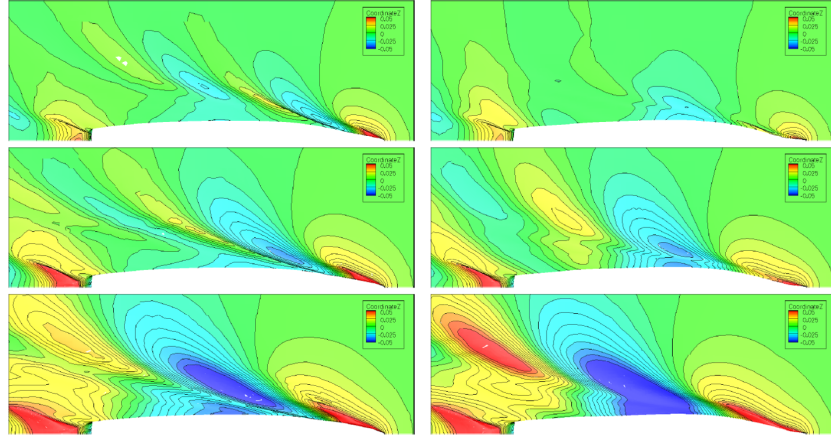


Fig. 13 RDO: wave patterns at slow, medium, and high speed for the baseline (left) and optimal (right) designs.

regions. The preliminary sensitivity analysis results (27 designs) are used as initial training set for the metamodel-based optimization. SRBF [25] is used in the present work. Gauss-Legendre quadrature and metamodel-based importance sampling have been used as UQ methods, as describe in Sec. IV.D.

Figure 15 shows the non-dominated solutions set provided by a deterministic version of the multi-objective particle swarm optimization algorithm [27]. No compromise solutions (capable to improve simultaneously both the objectives) are found, since the objectives are completely conflicting, as shown by the sensitivity results. Two designs optima are identified at the extrema (A and B) of the non-dominated solutions set and the corresponding hull stations are shown in Fig. 15. Total resistance expected value and operability improvement verification (by CFDShip-Iowa and SMP simulations, respectively) is shown in Fig. 16: design A provides about 3% improvement for the expected value of the

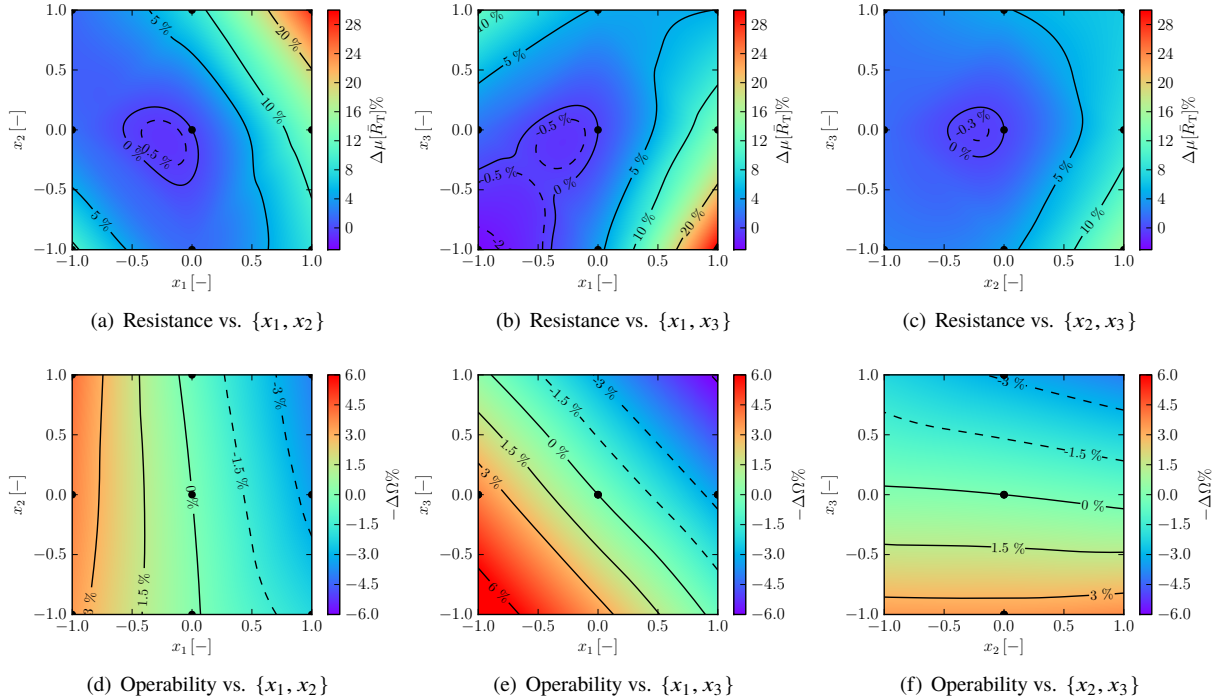


Fig. 14 RBRDO: preliminary sensitivity analysis.

total resistance in irregular waves with about 5% worsening of operability; design B shows 19% worsening for total resistance and about 8% improvement of operability.

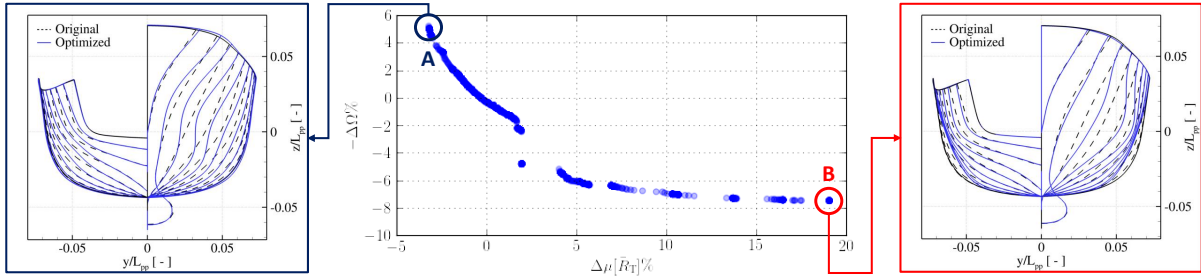


Fig. 15 RBRDO: non-dominated solutions set and optimal designs.

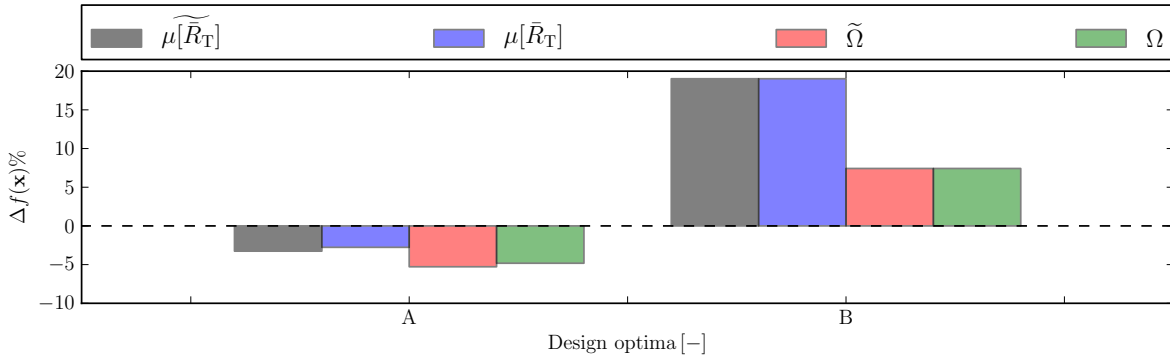


Fig. 16 RBRDO: verification of optimal designs. Comparison of objective functions metamodel predictions “~” and CFD verification.

VI. Conclusions

The design-space augmented dimensionality reduction method is based on KLE analysis and combines shape design modifications with the associated multi-physics performance for multiple design conditions, based on low-fidelity computations. Combining design modifications and performance improves the effectiveness of the design space dimensionality reduction for the subsequent design optimization by high-fidelity solvers (Fig. 1), has shown in [2, 3].

The method is demonstrated through the solution of RDO and RBRDO problems of a naval destroyer hull form, namely the DTMB 5415 model, subject to stochastic speed, sea state, and heading. Results are shown for improved resistance (in calm water and waves) and seakeeping performance. The RDO problem, by trading off high-speed performance for low-speed efficiency, produced a total resistance coefficient reduction of 4.4% over the speed range. The RBRDO problem, shows the complexity (for the current problem) of improving both total resistance and operability in waves, since no compromise solutions have been found. Nevertheless, significant objective improvements have been found at the extrema of non-dominated solutions set: about 3% for total resistance and 8% for operability.

The effectiveness and efficiency of the ADR method are affected, in general, by the nonlinearities involved in the process. In order to quantify their effects, ongoing research focuses on nonlinear extensions of the current methodology [28–30].

Acknowledgments

The work is supported by the US Department of the Navy Office of Naval Research Global, NICOP grant N62909-18-1-2033, administered by Dr. Salahuddin Ahmed and Dr. Woei-Min Lin, and by the Italian Flagship Project RITMARE,

funded by the Italian Ministry of Education. The research is performed within NATO STO Task Group AVT-252 “Stochastic Design Optimization for Naval and Aero Military Vehicles”.

References

- [1] Diez, M., Serani, A., Campana, E. F., Volpi, S., and Stern, F., “Design Space Dimensionality Reduction for Single- and Multi-Disciplinary Shape Optimization,” *17th AIAA/ISSMO Multidisciplinary Analysis and Optimization (MA&O), AVIATION 2016*, Washington D.C., USA, June 13-17, 2016.
- [2] Serani, A., Campana, E. F., Diez, M., and Stern, F., “Towards Augmented Design-Space Exploration via Combined Geometry and Physics Based Karhunen–Loève Expansion,” *18th AIAA/ISSMO Multidisciplinary Analysis and Optimization Conference (MA&O), AVIATION 2017*, Denver, USA, June 5-9, 2017.
- [3] Serani, A., and Diez, M., “Shape Optimization under Stochastic Conditions by Design-space Augmented Dimensionality Reduction,” *19th AIAA/ISSMO Multidisciplinary Analysis and Optimization Conference (MA&O), AVIATION 2018*, Atlanta, GA, USA, June 25-29, 2018.
- [4] Diez, M., Campana, E. F., and Stern, F., “Design-space dimensionality reduction in shape optimization by Karhunen–Loève expansion,” *Computer Methods in Applied Mechanics and Engineering*, Vol. 283, 2015, pp. 1525–1544.
- [5] Borzì, A., Schulz, V., Schillings, C., and von Winckel, G., “On the treatment of distributed uncertainties in PDE-constrained optimization,” *GAMM-Mitteilungen*, Vol. 33, No. 2, 2010, pp. 230–246.
- [6] Schillings, C., Schmidt, S., and Schulz, V., “Efficient shape optimization for certain and uncertain aerodynamic design,” *Computers & Fluids*, Vol. 46, No. 1, 2011, pp. 78–87.
- [7] Chen, X., Diez, M., Kandasamy, M., Zhang, Z., Campana, E. F., and Stern, F., “High-fidelity global optimization of shape design by dimensionality reduction, metamodels and deterministic particle swarm,” *Engineering Optimization*, Vol. 47, No. 4, 2015, pp. 473–494.
- [8] Serani, A., Fasano, G., Liuzzi, G., Lucidi, S., Iemma, U., Campana, E. F., Stern, F., and Diez, M., “Ship hydrodynamic optimization by local hybridization of deterministic derivative-free global algorithms,” *Applied Ocean Research*, Vol. 59, 2016, pp. 115 – 128.
- [9] Diez, M., Campana, E. F., and Stern, F., “Development and evaluation of hull-form stochastic optimization methods for resistance and operability,” *Proceedings of the 13th International Conference on Fast Sea Transportation, FAST 2015*, Washington, D.C., USA, 2015.
- [10] Diez, M., Campana, E. F., and Stern, F., “Stochastic optimization methods for ship resistance and operational efficiency via CFD,” *Structural and Multidisciplinary Optimization*, Vol. 57, No. 2, 2018, pp. 735–758.
- [11] Poole, D., Allen, C., and Rendall, T., “High-fidelity aerodynamic shape optimization using efficient orthogonal modal design variables with a constrained global optimizer,” *Computers & Fluids*, Vol. 143, No. Supplement C, 2017, pp. 1 – 15.
- [12] Diez, M., Serani, A., Stern, F., and Campana, E. F., “Combined Geometry and Physics Based Method for Design-Space Dimensionality Reduction in Hydrodynamic Shape Optimization,” *Proceedings of the 31st Symposium on Naval Hydrodynamics, Monterey, CA, USA*, 2016.
- [13] Queutey, P., and Visonneau, M., “An Interface Capturing Method for Free-Surface Hydrodynamic Flows,” *Computers & Fluids*, Vol. 36, No. 9, 2007, pp. 1481–1510.
- [14] Leroyer, A., and Visonneau, M., “Numerical methods for RANSE simulations of a self-propelled fish-like body,” *Journal of Fluids and Structures*, Vol. 20, No. 7, 2005, pp. 975 – 991.
- [15] Wackers, J., Deng, G., Guilmeneau, E., Leroyer, A., Queutey, P., and Visonneau, M., “Combined refinement criteria for anisotropic grid refinement in free-surface flow simulation,” *Computers and Fluids*, Vol. 92, 2014, pp. 209 – 222.
- [16] Huang, J., Carrica, P. M., and Stern, F., “Semi-coupled air/water immersed boundary approach for curvilinear dynamic overset grids with application to ship hydrodynamics,” *International Journal for Numerical Methods in Fluids*, Vol. 58, No. 6, 2008, pp. 591–624.
- [17] Mousaviraad, S. M., “CFD prediction of ship response to extreme winds and/or waves,” Ph.D. thesis, University of Iowa, Iowa City, Iowa, USA, 2010. URL <http://ir.uiowa.edu/etd/559>.

- [18] Meyers, W. G., and Baitis, A. E., "SMP84: improvements to capability and prediction accuracy of the standard ship motion program SMP81," Tech. Rep. SPD-0936-04, David Taylor Naval Ship Research and Development Center, September 1985.
- [19] Irvine Jr., M., Longo, J., and Stern, F., "Pitch and Heave Tests and Uncertainty Assessment for a Surface Combatant in Regular Head Waves," *Journal of Ship Research*, Vol. 52, No. 2, 2008, pp. 146–163.
- [20] Anderson, T., Gerhard, K., and Sievenpiper, B., "Operational Ship Utilization Modeling of the DDG-51 Class," *Proceedings of ASNE Day 2013 Symposia*, 2013.
- [21] Bales, S. L., "Designing Ships to the Natural Environment," *Naval Engineers Journal*, Vol. 95, No. 2, 1983, pp. 31–40.
- [22] Kennell, C. G., White, B. L., and Comstock, E. N., "Innovative Naval Designs for North Atlantic Operations," *SNAME Transactions*, Vol. 93, 1985, pp. 261–281.
- [23] Wunsch, D., Nigro, R., Coussement, G., and C., H., "Quantification of combined operational and geometrical uncertainties in turbo-machinery design," Proceedings of the ASME GT 2015, GT2015-43399, 2015.
- [24] Loeven, G. J. A., Witteveen, J. A. S., and Bijl, H., "Probabilistic collocation: an efficient non-intrusive approach for arbitrarily distributed parametric uncertainties," *45th AIAA Aerospace Sciences Meeting and Exhibit, AIAA Paper 2007-317*, Reno, Nevada, 2007.
- [25] Volpi, S., Diez, M., Gaul, N., Song, H., Iemma, U., Choi, K. K., Campana, E. F., and Stern, F., "Development and validation of a dynamic metamodel based on stochastic radial basis functions and uncertainty quantification," *Structural and Multidisciplinary Optimization*, Vol. 51, No. 2, 2015, pp. 347–368.
- [26] Bassanini, P., Bulgarelli, U., Campana, E. F., and Lalli, F., "The wave resistance problem in a boundary integral formulation," *Surveys on Mathematics for Industry*, Vol. 4, 1994, pp. 151–194.
- [27] Pellegrini, R., Serani, A., Leotardi, C., Iemma, U., Campana, E. F., and Diez, M., "Formulation and parameter selection of multi-objective deterministic particle swarm for simulation-based optimization," *Applied Soft Computing*, Vol. 58, 2017, pp. 714–731.
- [28] D'Agostino, D., Serani, A., Campana, E. F., and Diez, M., "Nonlinear Methods for Design-Space Dimensionality Reduction in Shape Optimization," *3rd International Conference on Machine Learning, Optimization, and Big Data, MOD 2017, Volterra, Italy*, 2017.
- [29] Serani, A., D'Agostino, D., Campana, E. F., and Diez, M., "Assessing the Interplay of Shape and Physical Parameters by Nonlinear Dimensionality Reduction Methods," *Proceedings of the 32st Symposium on Naval Hydrodynamics, Hamburg, Germany*, 2018.
- [30] D'Agostino, D., Serani, A., Campana, E. F., and Diez, M., "Deep Autoencoder for Off-line Design-Space Dimensionality Reduction in Shape Optimization," *56th AIAA Aerospace Sciences Meeting, SciTech 2018*, Gaylord Palms, Kissimmee, Florida, USA, January 8-12, 2018.